Science of Remote Sensing 5 (2022) 100039

Contents lists available at ScienceDirect

Science of Remote Sensing

journal homepage: www.sciencedirect.com/journal/science-of-remote-sensing

A bi-directional strategy to detect land use function change using time-series Landsat imagery on Google Earth Engine: A case study of Huangshui River Basin in China

Zhenyu Shen [a,b,c], Yafei Wang [a,b,*], Han Su [d,**], Yao He [a,b], Shuang Li [e]

[a] Key Laboratory of Regional Sustainable Development Modeling, Institute of Geographic Sciences and Natural Resources Research, Chinese Academy of Sciences, Beijing, 100101, China
[b] College of Resources and Environment, University of Chinese Academy of Sciences, Beijing, 100049, China
[c] College of Geographical Sciences, Qinghai Normal University, Xining, 810008, China
[d] Twente Water Centre, Faculty of Engineering Technology, University of Twente, Horst Complex Z223, P.O Box 217, 7500, AE Enschede, the Netherlands
[e] Center for Historical Geography Studies, Fudan University, Shanghai, 200433, China

ARTICLE INFO

Keywords:
Bi-directional detection
Google Earth Engine (GEE)
Time series
Land use function
Classification
Change detection
Urban expansion
Cropland loss
Watershed

ABSTRACT

Constructed land, cropland, and ecological land are undergoing intense competition in many rapidly-developing regions. One of the major reasons to cause frequent land use (LU) conversions is the policy dynamics. The detection of such conversions is thus a prerequisite to understanding urban dynamics and how policies shape landscapes. This paper presents a bi-directional strategy to detect the LU change of the Huangshui River Basin of China from 1987 to 2018 using time-series Landsat imagery. We first initialized classification and optimization of remote sensing images using the Random Forest algorithm; We then detected bi-directional spatio-temporal changes based on the distribution probability of land-cover types. Our results reveal complicated dynamics underlying the net increase in urban and built-up land (UB) and the net decrease in cropland. In this area, due to the implementation of ecological compensation projects such as ecological migration and mine restoration, we found that on average 5.52 km^2 of UB was converted into ecological land (forest, grassland and shrubland) every year, even though UB has expanded 3.6 times in the last 30 years with multiple conversions for cropland and ecological land. Meanwhile, 60% of lost cropland was converted to shrubland and grassland, and 40% was converted to UB. The accuracy of LU classification increases by 6.03% from 88.17%, and kappa coefficient increases by 2.41% from 85.16, compared to the existing initial results and uni-directional detection method. This study highlights the importance of the use of an effective remote sensing-based strategy for monitoring high-frequency LU changes in watershed areas with complicated human-nature interactions.

1. Introduction

Remote sensing technology has been proved to be a powerful tool in detecting rapid, macroscopic, and dynamic surface land use/cover changes (Turner et al., 2007; Cracknell, 2019; Feizizadeh et al., 2021a). Conflicts between urbanization, food production, and conservation of ecosystem diversity have become increasingly prominent along with the increase of human activities. These conflicts are highly dynamic due to the frequent policy-driven inter-landcover conversions, such as industrial development, cropland protection, and ecological conservation (Chen et al., 2021b). Thus, there is an increasing need for LU monitoring at high temporal and spatial resolutions (Wang and Gamon, 2019; Weiss et al., 2020; Zeng et al., 2020). Time-series images make it possible to detect high-resolution LU changes thanks to their rich temporal features able to reflect seasonality and long-term stability (Hütt et al., 2016; Wang et al., 2017; Thyagharajan and Vignesh, 2017; Bhosle and Musande, 2019; Zhang et al., 2020). With the development of remote sensing technology which provides various types and resolutions of remote sensing data, such as multispectral, hyperspectral, and microwave images, a wide application of time series images becomes possible.

* Corresponding author. Key Laboratory of Regional Sustainable Development Modeling, Institute of Geographic Sciences and Natural Resources Research, Chinese Academy of Sciences, Beijing, 100101, China.
** Corresponding author.
E-mail addresses: wangyafei@igsnrr.ac.cn (Y. Wang), h.su@utwente.nl (H. Su).

https://doi.org/10.1016/j.srs.2022.100039
Received 7 June 2021; Received in revised form 23 February 2022; Accepted 23 February 2022
Available online 25 February 2022

In 2008, Landsat data were made available to the public for free to download. It has greatly reduced the cost of acquiring historical remote sensing images. The question of how to make full use of the advantages of remote sensing images to improve LU monitoring has been arousing more and more attention (Cracknell, 2019).

At present, there are two main methods for LU change detection: post classification comparison or bi-temporal change detection, and temporal trajectory analysis. The former is based on the classification of mono-temporal images. It compares classifications of different time phases to detect changes, generally using anniversary dates or anniversary windows (annual cycles or their multiples). It emphasizes classification accuracy and algorithm research on a single image, including support vector machine (Mountrakis et al., 2011), random forest (Mutanga and Kumar, 2019), and various deep learning methods (Wu et al., 2021; Feizizadeh et al., 2021b; Garajeh et al., 2021), mostly for all land-cover types (Ibrahim et al., 2014). The advantage is that it can extract trending changes between land-cover types within a specific time period without requiring large computational time, but likely ignoring the details of the process. The latter usually reconstruct the ground-type evolution by constructing a time series index, using its seasonal and periodic characteristics, detecting time mutation points to obtain the transformation of target features, and paying more attention to intra-annual and inter-annual changes on a time series scale. Such as convolutional neural network (CNN) model method (Grings et al., 2020), break for additive season and trend (BFAST) model method (Verbesselt et al., 2010) and time series detection method based on NDVI time series (Yang et al., 2018). These methods can effectively capture the direction and time of transition between land types, and better reflect the law of land type transfer, but they mostly target single ground type (impervious surface, cropland, forest). They also need more computations and thus more suitable for small area research. For areas with a fragile ecological environment and a severe human-land conflict, in order to accurately reveal the complex transformation relationship between land types, it is necessary to combine the advantages of the two to carry out large-scale, long-term, high-frequency land cover classification and change detection. The recently developed Google Earth Engine (GEE, https://earthengine.google.com/) as a cloud platform makes this idea possible.

Surface cover monitoring studies with the GEE platform have achieved significant progress in detecting changes in single or specific features and specific phenomena, including impervious surface (Liu et al., 2018), cropland (Teluguntla et al., 2018), wetland (Mahdianpari et al., 2019), mangrove (Li et al., 2019a), industrial oil palm (Lee et al., 2016), drought assessment (Sazib et al., 2018), and flood monitoring (Beaton et al., 2019). Because of the excellent computational power and petabyte-level data catalog of GEE (Gorelick et al., 2017), monitoring long time series and high-frequency LU changes become feasible. For example, Hu & Hu (2019) used GEE to study the annual land change and its driving mechanism in Central Asia from 2001 to 2017; Khanal et al. (2020) studied annual LU in Province No.1 of Nepal for the period 2000–2018; Feizizadeh et al. (2021c) utilizes machine learning algorithms on the GEE for land use/land cover (LULC) mapping and change-detection analysis using a Landsat satellite image time series at an environmentally sensitive area in Northern Iran.

However, some issues on LU change and conflicts detection need to be addressed. First, the detection study of annual frequency needs to consider the logical problem of land-cover types development (Li et al., 2015; Zhang and Weng, 2016; Zhang et al., 2017). The general bi-temporal change detection studies, however, usually ignore the transition mode between different land-cover types consistent with realistic logic due to the long observation interval (5 years or more) (Tsai et al., 2018; Tian et al., 2014). Secondly, since LU transition is complex, it calls for new methods instead of being simplified by smoothing the whole land-cover types through a variety of periodic filtering methods (Khanal et al., 2020), which can only correct outliers in a reasonable range (Atkinson et al., 2012; Shao et al., 2016). Finally, bi-directional and multiple changes among cropland, forest, grassland, and constructed land are common in some areas due to the frequently-changing policies. For these types of regions, the above methods have limited accuracies of their classification and change detection.

Here we selected Huangshui watershed in China as a study area where multiple policies lead to frequent LU changes. The study area is located in the transition zone between Qinghai-Tibet Plateau and Loess Plateau, which is environmentally fragile and sensitive to both climate change and human activities (Ge and Zhang, 2017; Yang and Liu, 2013). It is also the focus of China's "Grain to Green" and "the Great Western Development" policies. There is competition among urban expansion, grain demand, and ecological conservation, due to the economic and population agglomeration (Jia et al., 2020). There are bi-directional and multiple transformations among cropland, forest, grassland, and construction land. In an ecological transition area with a complex topography and drastic changes like Huangshui River Basin in China, it is a challenging task to carry out high-frequency long time-series remote sensing detection for the whole land-cover types. In this study, we present a bi-directional strategy to detect LU annual changes based on the classification of time series Landsat imagery. We then carried out and validated them on Google Earth Engine platform. Based on the statistics of the classification and the detection results, we further analyzed the patterns of changes in different land-cover types.

2. Study area and datasets

2.1. Study area

The Huangshui River Basin is located in the northeastern Qinghai Province, China, and in the transition zone between the Loess Plateau and the Qinghai-Tibet Plateau (36°02'~37°28' N, 100°42'~103°04'E), with a drainage area of about 16,200 km^2. The combination of Huangshui mainstream area and its tributary Datong River Basin is a special physiographic unit being wide in the west and narrow in the east, and is also unique ecosystem in the Qinghai-Tibet Plateau (Dong et al., 2021). The basin presents a pinnate drainage pattern, with high-northwest and low-southeast landscapes. The mainstream flows from the northwest to the southeast. The basin includes river valleys, plains, loess hills, alpine pastures, and middle & high mountains, with a minimum altitude of 1, 655 m, a maximum altitude of 4,860 m, and a sharp vertical difference (Fig. 1). The total area of the Huangshui River Basin only accounts for 2.24% of the area of Qinghai Province. The population, industrial and agricultural production value account for more than 50% of the entire Qinghai Province, as it is the most densely populated and economically developed area in Qinghai Province. The Huangshui River Basin has an annual precipitation of 300–500 mm. It locates in an arid and semi-arid climate zone and is an ecological transition zone with precipitation of 400 mm and a typical agricultural and pastoral transition zone in China. The population is constantly converging, and urban expansion and cropland protection compete in a limited space (Jia et al., 2020). The agricultural and pastoral transition zone itself is extremely ecologically fragile and is a policy area for the "Grain to Green" program under the leadership of the Chinese government (Zhao et al., 2020). The competition between cropland production and the protection of ecologically fragile areas is extremely prominent.

2.2. Datasets

We mainly used Landsat series image, including Thematic Mapper (TM), Enhanced Thematic Mapper Plus (TEM+), and Operational Land Imager (OLI) data. Data in the following two periods was considered in order to obtain the maximum vegetation spectral difference, including the greening (June–October) and browning periods (November - next March). We calculated spectral indices such as Normalized Difference Vegetation Index (NDVI), Normalized Difference Water Index (NDWI), and Normalized Difference Built-up Index (NDBI). To obtain as many

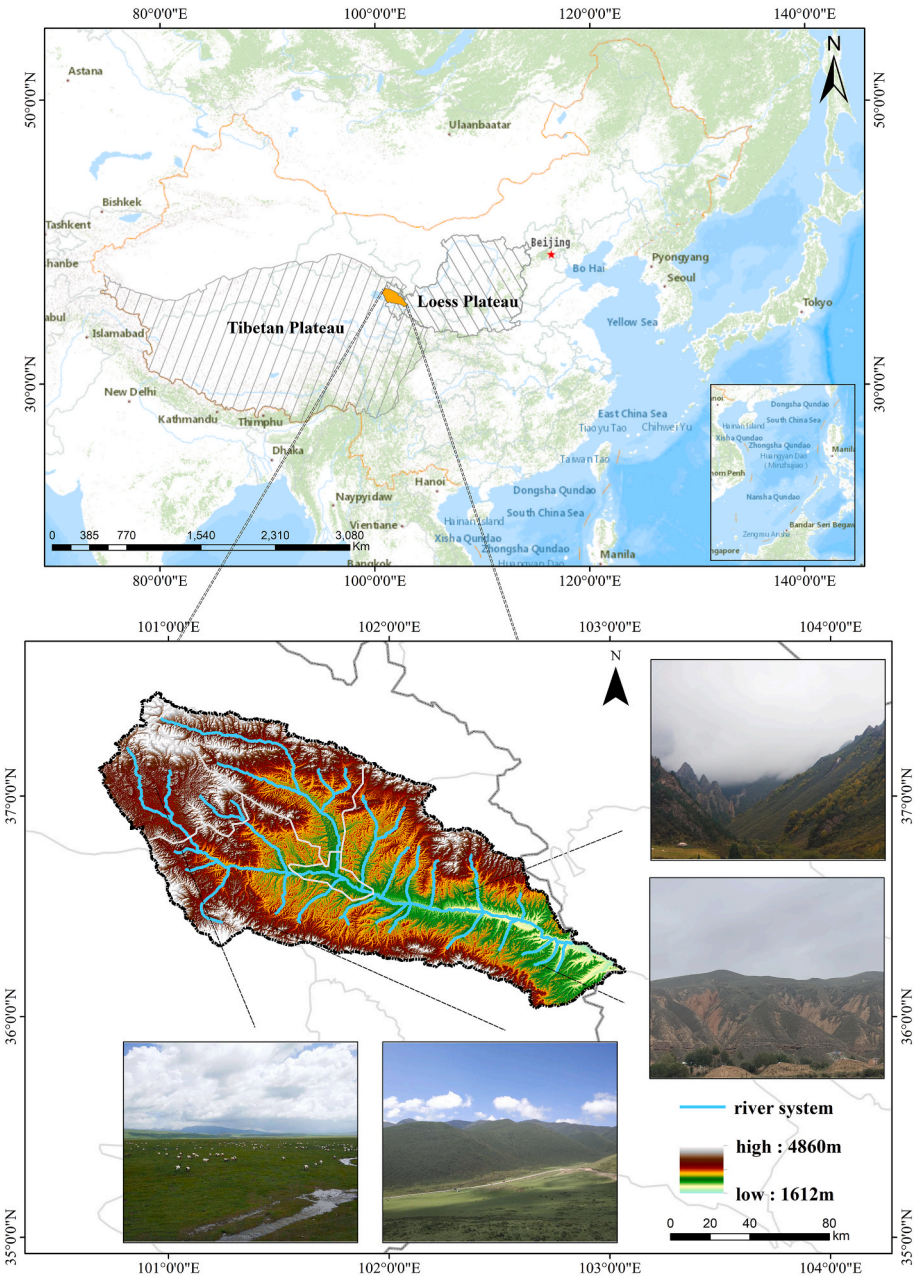

Fig. 1. Study area and field study route.

annual observational data with cloud cover less than 10% as possible, a total of 24-year low-cloud cover data from 1987 to 2018 were obtained through image acquisition based on pixel mosaic (Li et al., 2019b), which is 6 years longer than the entire scene mosaic. Auxiliary data for classification included night light data, digital elevation data, and climate data. Among them, the night light data (nighttime day/night band composites version 1) was used to distinguish urban and non-urban areas and provides monthly average radiation composite images of visible infrared imaging radiometer suite (VIIRS) day/night band (DNB) night data. The digital elevation model was retrieved from the Land Processes Distributed Active Archive Center (LP DAAC) (the United States) and has been filled with open-source data (ASTER GDEM2, GMTED2010, and NED) (Farr et al., 2007). Climate data was from Famine Early Warning Systems Network (FEWS NET) Land Data Assimilation System (FLDAS). It includes climate-related variables, i.e., moisture content, humidity, evapotranspiration, average soil temperature, and total precipitation rate (McNally et al., 2017). In addition, the China meteorological dataset is obtained from the Resource and Environmental Science and Data Center of the Chinese Academy of Sciences, which includes meteorological variables such as Pa (annual average precipitation), TaDEM (annual average temperature), and AAT10DEM (accumulated temperature $\geq$10 °C). The dataset is based on meteorological data from 1915 stations in China, including monthly precipitation and monthly average temperature from each station for many years. Pa, TaDEM, and AAT10DEM are calculated based on the station data after altitude correction, and the national spatial distribution dataset was interpolated through inverse distance weighting average (Xu and Zhang, 2017). Table 1 is the data details.

2.3. Classification system and sampling

According to previous studies on LU classification systems in the basin (Cao et al., 2020), this paper builds a LU classification system consisting of 7 types, i.e., cropland, shrubland, forest, grassland, water,

Table 1
Details of the data source.

DATA	Year (s)	Spatial Resolution	Temporal Resolution
Landsat[a]	1987–2018	30 m	16 days
NPP/VIIRS[a]	1992–2018	15 arc seconds	1 month
STRM[a]	2000	30 m	–
FLDAS[a]	1982–2018	0.1°	1 month
Pa (Average annual precipitation)	1990–2018	500 m	–
TaDEM (Annual average temperature)	1990–2018	500 m	–
AAT10DEM (≥10 °C accumulated temperature)	1990–2018	500 m	–

[a] Is online access to data through the GEE platform.

urban and built-up, and bareland. Table 2 is for specific ground objects.

3. Methods

For long time-series and high-frequency LU change detection using remote sensing images, it is challenging to reduce classification errors and their impacts on change detection. To address this challenge, we present a bi-directional strategy to detect the LU change using time-series Landsat imagery, which mainly includes the initial classification using continuously optimized random forest and the bi-directional spatial-temporal consistency detection method. The following sections describe each individual component of the whole process in detail (Fig. 2).

3.1. Sample library establishment and validation

The quality of training samples directly affects the final classification results (Xie et al., 2019). Establishing historical images is indeed a challenging task. We conducted a detailed field investigation and adopted a robust site selection strategy. We first set up a total of 20 days of field visits in the study area in 2017 and 2018 to more intuitively understand the geomorphology and land-cover types distribution of the study area. Then, the whole 24-year sample data were obtained by backward modification year by year and point by point. The training sample of 2018 was obtained by using the high-resolution images combined with the fieldwork understanding. For the training sample of 2017, we looked at historical images of 2017 and checked whether the ground type have changed point by point. Based on this approach, we gave category replacement and deletion adjustment to the samples. Since there are no high-quality images for reference on Google Earth before 2000, this process involved not only information from historical images, but also experience from field visits and local knowledge obtained from local residents during field visits. In this way, we obtained training samples backward to the year 1987. This sample selection strategy ensures the continuity and stability of the sample selection process as much as possible. 80% of the samples were used as training samples and 20% were used as validation samples.

Table 2
Feature classification system.

Category	Abbreviation	Description
Cropland	CRL	Refer to land used for growing crops
Shrubland	SRL	Refer to shrubland and scrubland with canopy density >40% and height below 2 m
Forest	FRT	Refer to natural and man-made forests with canopy density >30%
Grassland	GRL	Natural grassland and improved grassland
Water	WTR	Natural inland water and land for water conservancy facilities
Urban and built-up	UB	Refer to urban and rural residential areas and land for industry, mining, transportation, etc.
Bareland	BRL	Land not yet used, including barren land

Accuracy evaluation through confusion matrix and two indicators of completeness rate and correctness rate are selected. The completeness rate is the ratio of the number of pixels obtained by a certain land type classification to the total number of actual pixels of the land type, corresponding to the missing points; the correct rate is the number of pixels correctly classified divided by the actual number of land types to the total number of pixels, corresponding to the misclass points.

3.2. Initial classification using continuously optimized random forest

An essential prerequisite for a bi-directional spatial-temporal consistency detection strategy is to obtain the initial classifications with as high accuracy as possible. The random forest (RF) classifier, comprised of a decision-tree classification using the bagging strategy and an internal algorithm on the GEE platform (Xie et al., 2019), was used to combine the training data and composited metrics for land-cover mapping. It has advantages in relatively robust performance, the capability of the inclusion of a bigger number of variables, and quantitative measurement of variable contributions (Belgiu and Drăguţ, 2016).

Firstly, in terms of supervised classification, classification results were greatly affected by the distribution of training samples (Foody and Mathur, 2004). Especially for research areas with fragmented landscape and strong spatial heterogeneity, the accuracy of the final results was directly affected by the distribution of training samples which needs to contain complete and comprehensive surface features (Long et al., 2018). Therefore, training data were randomly sampled 10 times based on random functions of the GEE platform, and the results with maximum accuracy were taken as the optimal sample point distribution. Secondly, texture is an essential feature for remote sensing images. Through texture analysis, hidden information can be obtained from the images by extracting spatial changes (Jin et al., 2018; Franklin, 2020). Unlike color features, the texture is not pixel-based, but region-based. The detection window for texture analysis is carefully designed in this study considering the following contradictory impacts: The larger detection window, the stronger ability to detect spatial consistency, but a small detection window can accurately locate the texture's abrupt change. Thus, we dynamically set the window size to 1–9 according to the image quality each year to select the most accurate texture and its corresponding optimal window size. In addition, since this area is a typical ecological transition zone, climatic conditions on the one hand are deemed as the main driving factors affecting the change of LU pattern in this area (Zhang et al., 2020). On the other hand, previous studies demonstrated that landcover types such as grassland, shrubland, and forest could feedback the influences of precipitation changes. Accordingly, this paper introduced precipitation, soil moisture, temperature, and other climate factors to facilitate classification and improve classification accuracy (Cui et al., 2021). After the above optimization, the initial classification accuracy could be gradually improved. Taking 2018 as an example, the minimum initial accuracy of optimized results increased from 79.01% to 86.33%, 87.13%, and 87.21% respectively, with a remarkable increase of 7.32% at the stage of optimizing the sample point distribution.

3.3. The bi-directional spatial-temporal consistency detection method

We assumed that the conversion between different land-cover types generally presents certain continuity and rationality. Specifically, when one land-cover type undergoes a relatively stable period, then other types occasionally appeared within this process is likely incorrect. Therefore, our method is to improve the accuracy of the results by modifying the intrusive types caused by classification errors that destroy the dominant type during the stable period. Its main steps are as follows:

(1) Eliminate the outliers in the time dimension for stable land-cover types. In each time series, we consider that the isolated ground pixels are unreasonable and regarded as a classification error. A

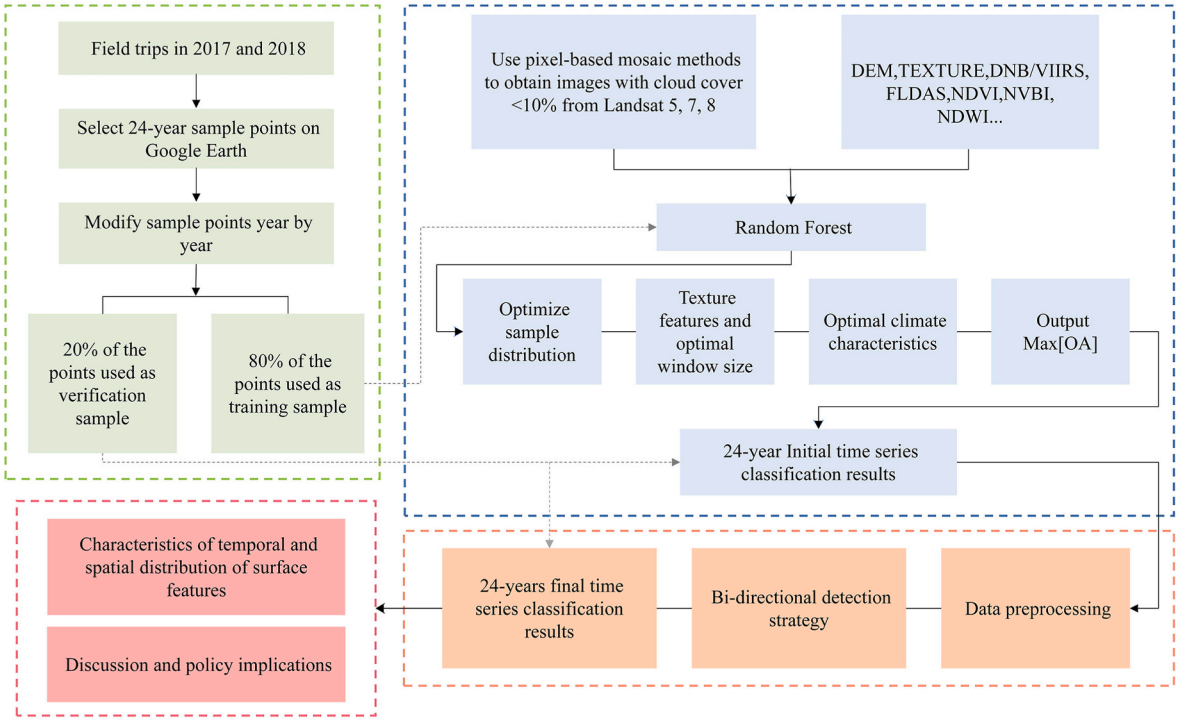

Fig. 2. Flowchart of the proposed bi-directional strategy to detect land use change.

time filter method (Li et al., 2015) is used to eliminate those noises and modify time series.

(2) Bi-directional window consistency correction. Two initial seed windows are built up on both sides of the time series of the classification results, and two detection windows are created in the front of the seed window. The consistency of the ground types between initial seed windows and detection windows is judged by using formula (1), and the correction process is simultaneous until the detection windows on both sides meet the loop stops (Fig. 3).

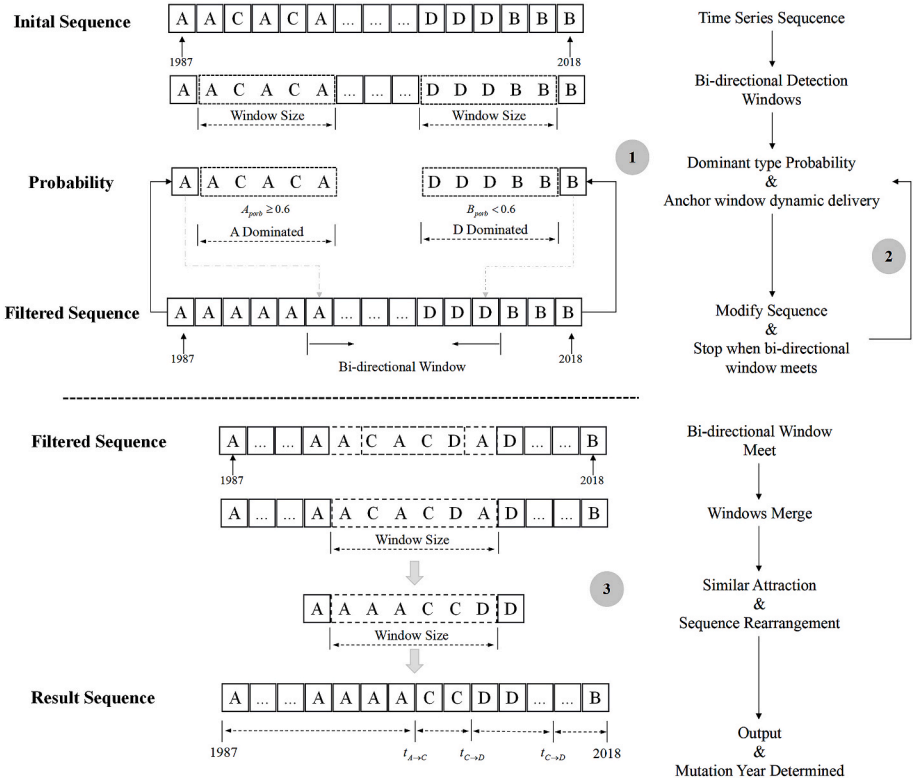

Fig. 3. Three-stage schematic diagram of the bidirectional spatial-temporal consistency detection method.

$$prob = \frac{\sum_{j=i+1}^{j=i+d} \mathrm{count}(W_i = W_j)}{W_d} \quad (1)$$

$$\begin{cases} W_s = W_{d(prob \geq 0.6)} \;\; L_{i+1} \rightarrow L_{j(i+1<j \leq i+d)} = K_s \;\; and \;\; s = j \\ W_s \neq W_{d(prob \geq 0.6)} \;\; s = s+1 \end{cases} \quad (2)$$

where W_s and W_d are seed window and detection window, and L_i and L_j are starting and ending cell of detection windows; K_s is the ground type of seed window, and K_d is the dominant ground type in a detection window; *prob* is the distribution probability of a ground type in the detection window. Taking a single side as an example, we need to determine whether the type K_s in W_s is identical with the dominant ground class K_d or not. For the former case, the algorithm will correct non-dominant ground class as dominant ones in W_d, move forward the seed window W_s to dominant ground type at the final position of W_d, and start next detection; for the latter case, it will move forward W_s only one position, and check W_d for consistency again. Determine dominant ground objects are which comparing the distribution probability and greater than the threshold 0.6 and vice versa (see formula 2).

(3) Identification of change nodes in time series of different land-cover types. When two detection windows meet, the algorithm stops. Both detection windows are merged into a large window, where types inside are resorted. Then, the years of ground types transfer are specified (see formula 3).

$$\begin{cases} n_1 = count(W_N = W_{ls} \;\;) \;\; W_{l(l=l+n_1)} \\ N = n_1 + n_2 + \ldots + n_n \\ n_2 = count(W_N = W_{rs} \;\;) \;\; W_{r(r=r-n_2)} \end{cases} \quad (3)$$

where N is the total number of pixels in a merged windowW_N; n_1 is the ground type inW_N which is identical with left cell W_{ls}; n_2 is the ground type in W_N which is identical with right cell W_{rs}; *count()* is a conditional function. When the ground type on the left and right of the equal sign are identical, it equals 1, otherwise equals 0. Finally, the left ground type W_l locates in $l+n_1$, the right ground type W_r locates in $r-n_2$, If there is an extra cell, another ground type will be filled. When ground types on both sides are un-identical, it is a year for a sudden change in ground type transformation.

4. Results

LU classification results for 24 years (1987–2018) based on the bi-directional strategy are shown in Fig. 4. We found that UB is gradually filling the entire valley area and expanding along its shores. The slopes of the valley and other small watersheds with large areas of cropland are gradually being occupied by UB. Other areas are covered in shrubland, forest, and grassland. Further comparative analysis of the classification results of different years shows that, firstly, UB is the fastest-growing class, increasing from 307.47 km^2 in 1987 to 1091.83 km^2 in 2018, an expansion of 3.6 times. Cropland is the main source of UB expansion, with a total area of 559.47 km^2, accounting for 67.51% of the total new UB growth. Forest, grassland, and other vegetation land account for 24.60%, followed by cropland. Secondly, cropland loss involves maximum area change, and cropland area was decreased by nearly 20% from 6114.09 km^2 in 1987 to 4900.33 km^2 in 2018. Among them, 827.12 km^2 cropland was converted into ecological land (includes forest, shrubland, and grassland), accounting for 59.09% of the total lost area, much higher than 39.97% for UB, significantly different from the situation that cropland losses are mainly caused by the urban expansions in Eastern and Central China. Thirdly, ecological land such as forests and grassland presented a slow-growth trend, with an annual growth of 0.23% from 12,521.49 km^2 to 13,427.68 km^2.

Through analysis of conversion time for different types, it can be found that the LU change in this basin presents typical stage characteristics (Fig. 5). Firstly, the rate of UB expansion in different stages is significantly different. The newly added UB mainly occurred in 2000–2014, accounting for 56.54% of the total area. Among them, the annual average growth rate was 3.84% from 2000 to 2010, and quick expansion occurred in 2010–2014, with an annual average growth rate

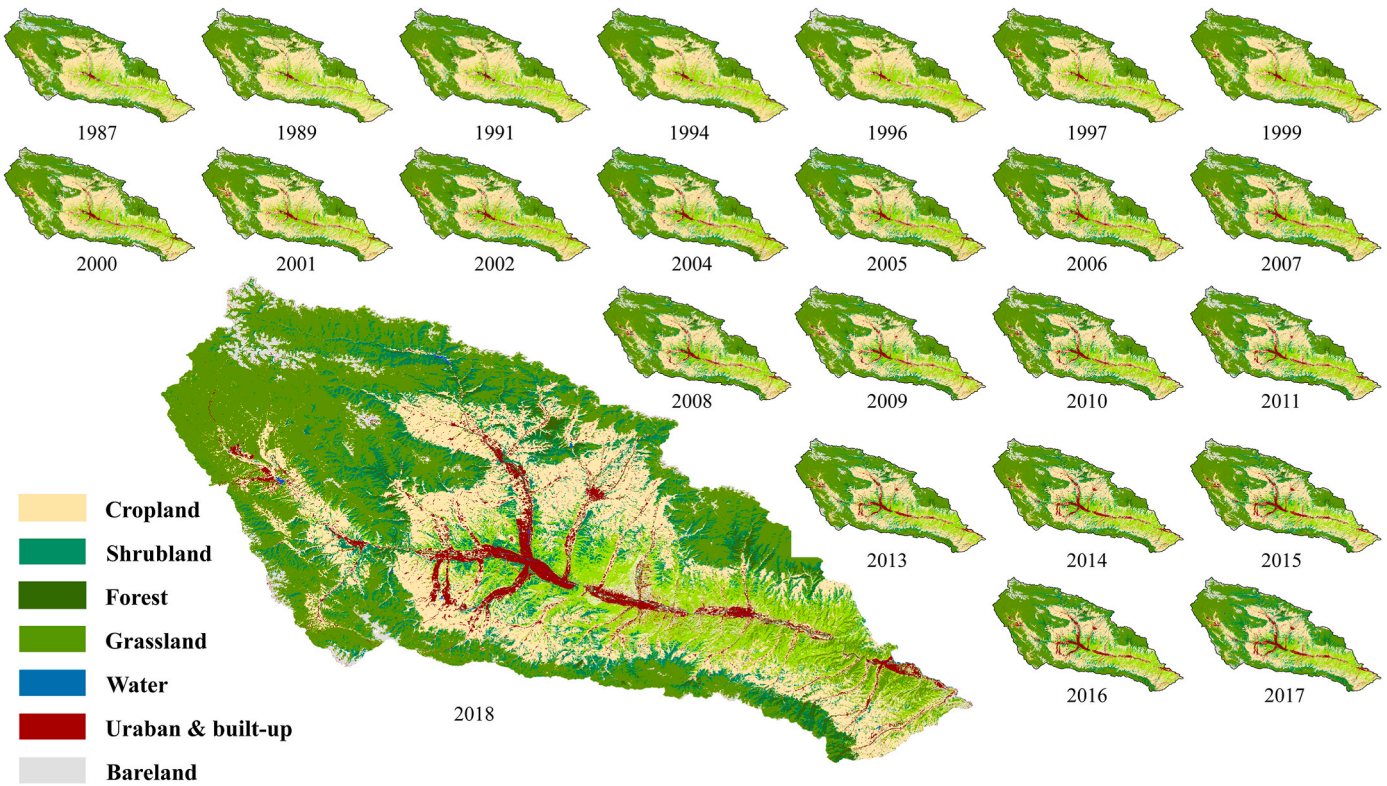

Fig. 4. Results of land use classification in Huangshui watershed from 1987 to 2018.

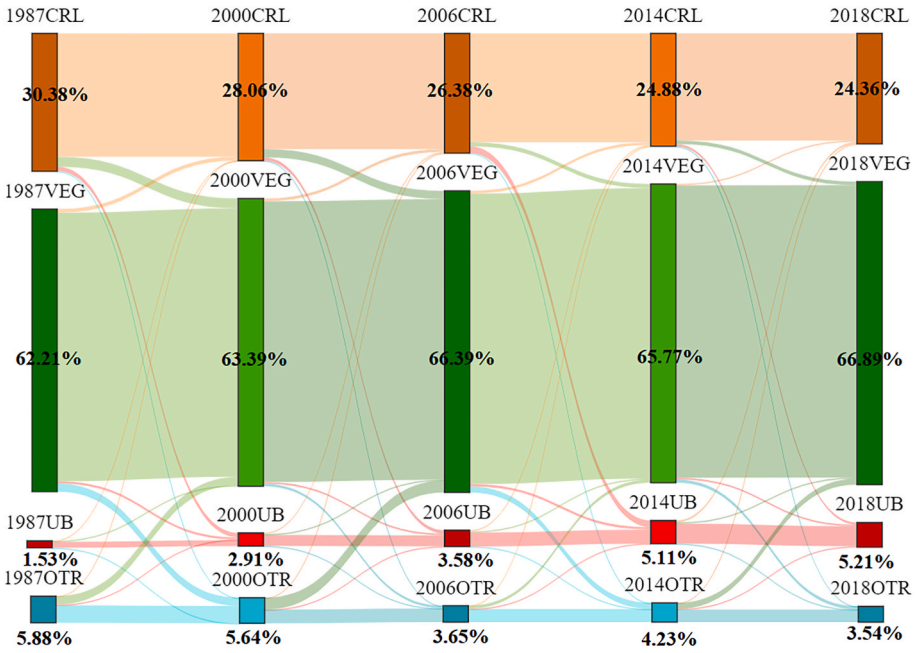

Fig. 5. Conversion matrix between different features at different stages in the Huangshui Basin from 1987 to 2018.

of 6.74%, more consistent with the "Great Western Development" program formulated by the Chinese government. Secondly, these are stage dominant characteristics during the processing when UB and ecological land invaded cropland. During 2000–2006 and 2014–2018, more cropland was converted into ecological land. In 2000–2006, 6.42% of cropland (362.30 km^2) was converted into ecological land, with an annual loss rate of 60.38 km^2/year, In 2014–2018, 3.20% of cropland (160.21 km^2) was converted into ecological land, with an annual average loss of 40.05 km^2/year, accounting for 76.00% and 65.40% of the cropland loss respectively, closely related to two rounds of "Grain to Green" program implemented by the Chinese government in 2000 and 2014. However, during 2006–2014, more cropland was converted to UB 0.5.61% cropland (298.16 km^2) was converted to UB, with an annual average loss of 37.27 km^2/year, accounting for 47.71% of cropland loss, much higher than 23.14% and 34.03% in other periods, and occupation of cropland for UB development was faster than returning cropland to ecological land. In general, UB expansion was dominant in 1987–2000 and 2006–2014, while returning cropland to ecological land was dominant in 2000–2006 and 2014–2018.

In addition, while rapid urbanization and the "Grain to Green" program are invading cropland in both directions, there is also a phenomenon that cropland reversely invades ecological land and UB. In the periods of 1987–2000, 2000–2006, 2006–2014, 2014–2018, there were 165.19 km^2, 129.16 km^2, 119.47 km^2 and 63.01 km^2 ecological land converted into cropland, and 38.70 km^2, 39.17 km^2, 45.04 km^2 and 48.42 km^2 UB converted into ecological land, respectively. The main reason for cropland conversion lied in that more rural laborers migrated out, and more cropland should be cultivated around large counties and urban areas to meet people's daily lives in the context of rapid urbanization (Hu et al., 2020). While for the latter, the "Grain to Green" program specifies ecological migration in remote rural areas unsuitable for farming and living, leading to houses collapse naturally and ecological restoration (Xu et al., 2020; Peng et al., 2020). This method has the advantage of accurately identifying the type of land involved in bi-directional conversion.

5. Discussion

5.1. Overall accuracy comparison analysis

One purpose of this study is to solve the logical errors that may occur in the time series. Most long-term LU change studies based on GEE (Tsai et al., 2018; Hu et al., 2019; E. Nyland et al., 2018) generally do not exist or do not consider the correction of logical errors. While some researchers have paid attention to the logical errors that may occur in long-term, high-frequency land change detection, their common feature is a focus on specific logical changes in specific features or phenomena, such as an impervious surface (urbanization process) (Li et al., 2015), cropland expansion (Jin et al., 2019), deforestation (Grings et al., 2020). These methods are all based on uni-directional and irreversible judgment logic. This motivate us to compare the proposed bi-directional detection method with the above two types of methods, i.e. the initial classification and uni-directional detection methods.

We compared the results for the years 1991, 1994, 1996, and 1999 to understand how the bi-directional method achieves higher accuracy (Fig. 6). To this end we normalized the area of cropland, grassland, and UB in the region and plot them as line graphs to show their area fluctuations under the three different results. We found that the initial results of cropland and grassland have a strong interannual variability, reaching 0.24 and 0.23, while the UB in 1994 shows an obvious logical error. Both the uni-directional and bi-directional methods have good correction effects. For example, the inter-annual variation of cropland and grassland is less than 0.05, and the UB also shows a monotonic increasing trend, which is in line with the actual situation. However, we also found that the area fold lines of some types of the uni-directional algorithm are too smooth. We found that the uni-directional method caused the situation in which strong type encroached on weak type, for example, the expansion of the cropland caused the discontinuous river and the forest on both sides to be missed in Fig. 6a; since the over-encroachment of the cropland, the grassland loses its typical geographical distribution characteristics that grows only on the shaded slope surface (water is not easy to evaporate) in the loess hilly area in Fig. 6c, while the bi-directional method effectively avoids this situation (Fig. 6b and d) (Zhao et al., 2020; Chen et al., 2021a).

We further compared our bi-directional method with the existing

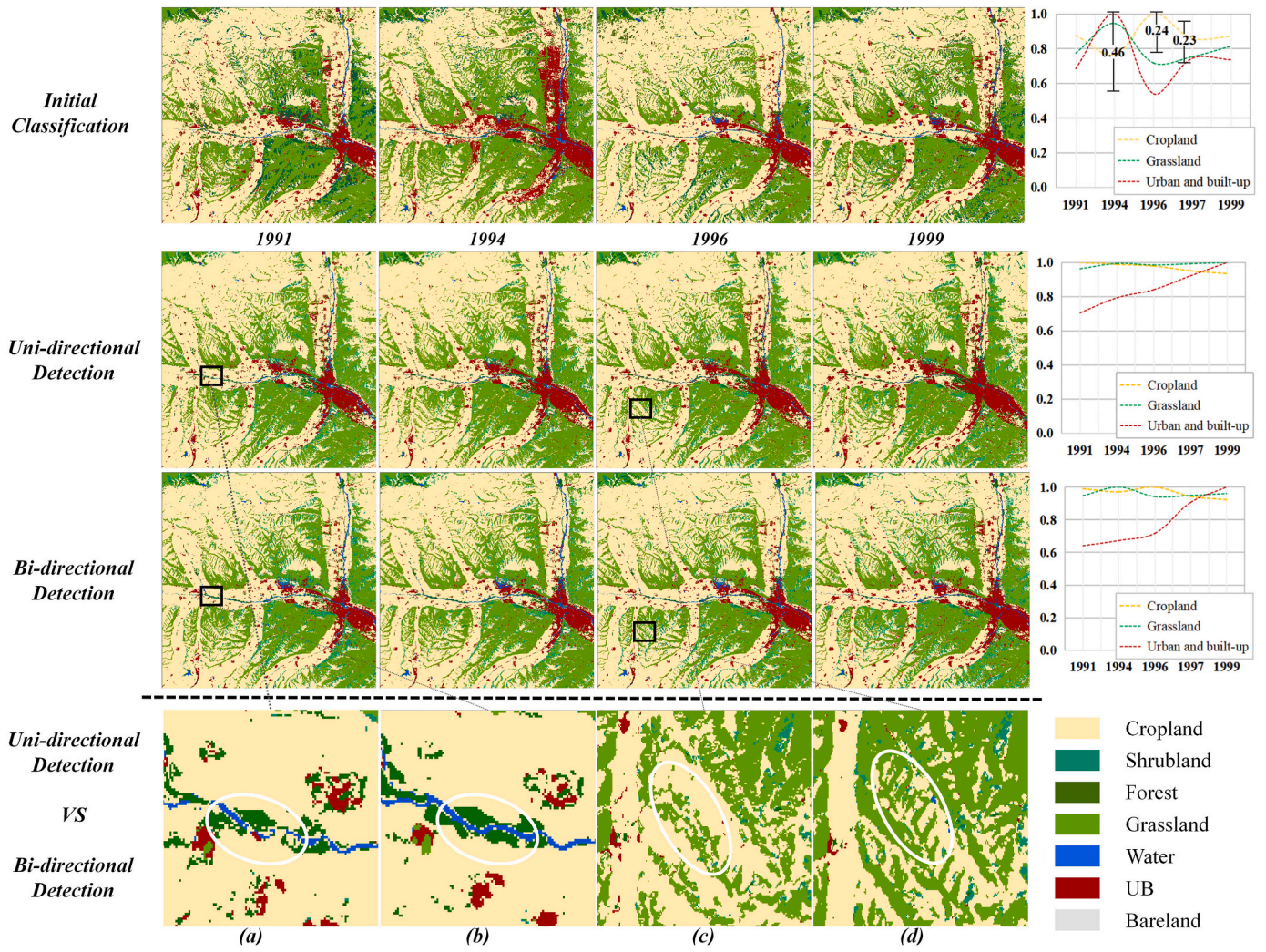

Fig. 6. Comparison of results for initial classification, uni-directional method, and bi-directional method.

initial classification and uni-directional method. Results show the bi-directional detection method was significantly better than initial classification and uni-directional detection in terms of overall change detection accuracy, and the average of the overall accuracy (OA) was increased by 6.03% and 2.41% respectively (Fig. 7a). The accuracy was improved to a different extent in different years, and the overall classification accuracy was improved significantly in some years. Compared with the initial classification results, accuracy improvement ranges arrange between 0.92% and 10.22%, the OA was most significantly improved in 2006, 2009, and 1996 with increases of 10.22%, 10.00%, and 9.17%, respectively. Compared with the uni-directional detection method, accuracy improvement ranges between 0.80% and 4.98%. The OA was most significantly improved in 2009,1991, and 2006 with increases of 4.98%, 4.51%, and 4.50%, respectively. In general, the OA of initial classification results was between 76.38% and 87.90%, and the average of OA was 82.14%; the OA of uni-directional detection results was between 81.53% and 90.49%, and the average of OA was 85.76%. The OA of bi-directional detection results was between 84.20% and 91.74%, and the average OA was 88.17%.

5.2. The correctness and completeness analysis of change detection

To comprehensively evaluate the method, the validation procedure was carried out both forwards and backwards. Forward validation is to assess the correctness of LU change detection using the proposed method, and backward validation is to evaluate the completeness of LU change detection. The correctness and completeness characterized the accuracy of change detection, and the advantages of this method were further illustrated. Different from the previous studies focusing on a single type (Chai and Li, 2018; Jin et al., 2019), this study has carried out a spatial-temporal consistency strategy for all land-cover types, drawn a radar chart to show the completeness accuracy (Fig. 7b) and correctness accuracy (Fig. 7c) of the initial classification, uni-directional detection and bi-directional detection results of 7 types of ground classes from 1987 to 2018.

The completeness accuracy of the cropland in the uni-directional results is 96.21%, which is much higher than 81.14% and 91.28% of the initial classification and bi-directional method, mainly because the cropland processed by the uni-directional method has the phenomenon of expanding and encroaching on other features, resulting in high completeness, while the results of the bi-directional method improve the original cropland classification accuracy while correcting the over-expansion of the uni-directional method to get a better result (Fig. 6a and c). As shown in Fig. 7b, the three methods of completeness accuracy for UB were 89.14%, 91.41%, and 91.51%, which did not improve significantly and did not exceed 2%, indicating that more misclassification occurred for UB during the whole time series. In addition, for shrubland, both uni-directional and bi-directional detection method improved their completeness well, improving the initial result of 53.12% with an increase of about 10%.

The correctness accuracy of the three methods of cropland is 80.60%, 81.20%, and 85.25%, especially the bi-directional method is improved

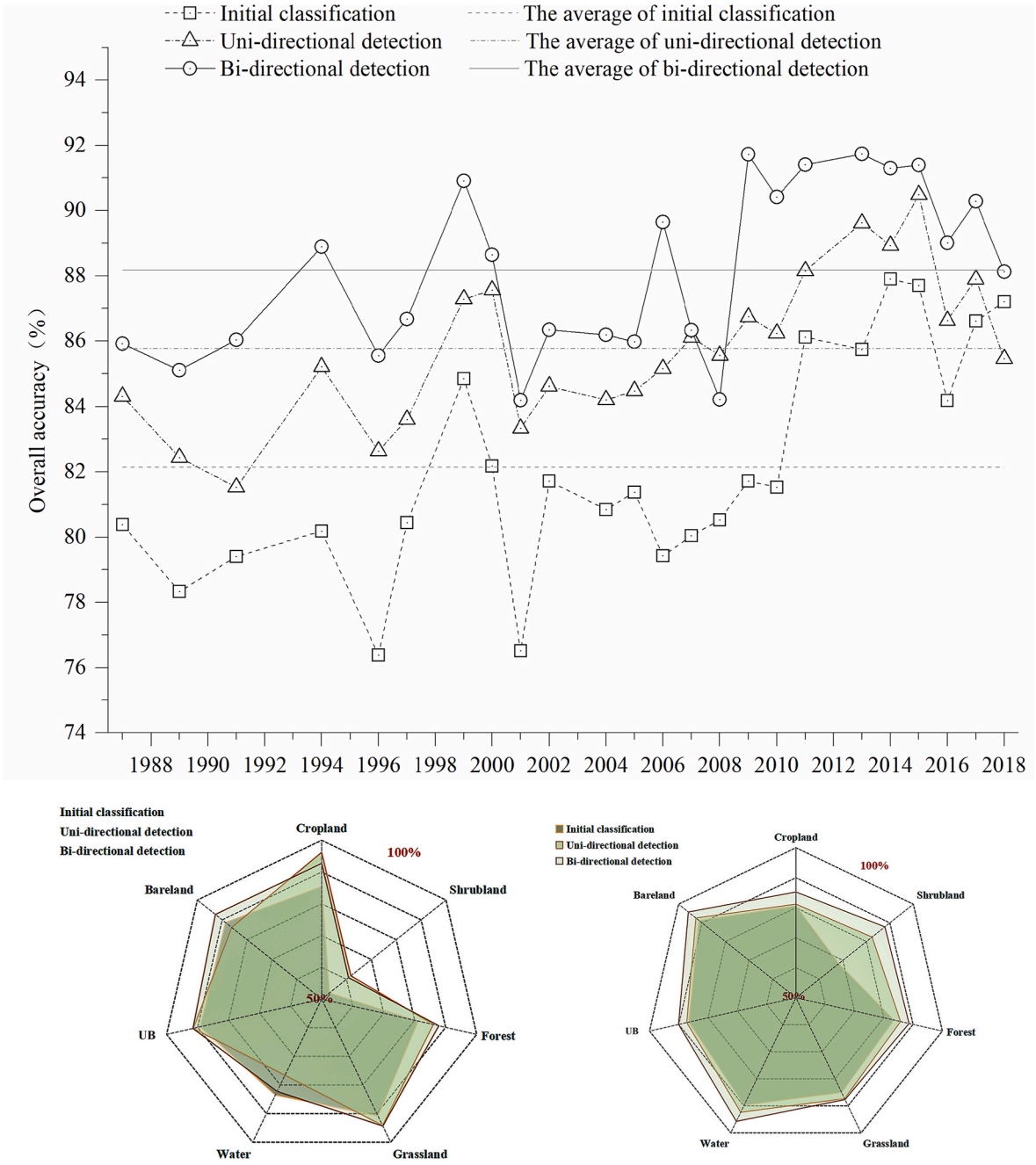

Fig. 7. Accuracy comparison of initial classification, uni-directional method and bi-directional method; (a) overall accuracy; (b) completeness accuracy; (c) correctness accuracy.

more, which is a good correction of the uni-directional method of the expansion of the score and improve the correctness (Fig. 6b and d). The correctness of shrubland has been improved more than the completeness, and the accuracy of the three stages are 68.22%, 82.43%, and 87.88%, respectively. Whether it is spectral or textural characteristics, shrubland are more likely to be confused with other surrounding types (Xie et al., 2019). Combined with the completeness rate, it can be found that the results processed by the bi-directional detection can well solve the problem of missing classification of shrubs on long-time series from a logical point of view.

5.3. Uncertainty and potential solutions

For long-time and high-frequency LU change detection studies, it is essential to correct the classification results using time-series contextual information. When the image density increases and the image quality decreases, it could lead to an exponential increase of errors and uncertainties in the LU classification of each period and the final change detection (Bruzzone and Prieto, 2000; Coppin et al., 2010; Feizizadeh et al., 2021a). Our experimental results show that this situation can be effectively improved by introducing contextual information. For example, cloud pollution and areas of bad image elements can be approximately replaced by results from neighboring years; the plausibility of transitions among types can be reasoned based on temporal contextual information.

As with many other similar methods, our strategy has a high dependence on the accuracy of the initial classification results (Smits and Annoni, 2000; Grings et al., 2020). We also acknowledge that a

certain amount of data redundancy is generated in providing feature vectors to the random forest classifier, and the feature vectors with high relevance should be selected for it to be trained to speed up the process and efficiency (Zhang and Yang, 2020; Belgiu and Drăguţ, 2016). In addition, our study area is located in an ecological transition watershed area, where features are confusing and difficult to classify, so a smaller detection window and a distribution probability threshold with low constraint are used. If for some regions with strong ecological resilience and high intensity of human activities, such as the developed areas of eastern China, where low elevation plain area with obvious and single land-cover types, a larger detection window and a higher distribution probability threshold can be adopted to obtain better results. Finally, in order to further optimize and improve the results, we need to consider the more sequential probability of feature distributions, especially the change characteristics of the time dimension of typical features and conduct experiments on larger areas of complex regions to test the stability of the strategy.

6. Conclusion

We proposed a bi-directional strategy to detect LU change for the Huangshui watershed, China, to achieve long time series and high frequency LU cover classification and monitoring for1987-2018. The most important feature of this method is that by judging the distribution probability of land types, complex topography, ecological transitions, and dramatic LU changes due to multiple regional policy influences can be identified. In our study this strategy significantly improves the classification accuracy with an annual average of overall accuracy of 88.17%, increased by 6.03% and 2.41%, respectively, compared with initial results and uni-directional detection method. This helps detect bi-directional spatial and temporal changes in LU and to explore how policy affects LU. Therefore, we believe that the temporal and spatial dimensional information embedded in the remote-sensed time series images should be fully considered and utilized in conjunction with the actual situation of the region, and these will effectively enhance the quality of the LU classification and change detections for climate-sensitive and environmentally fragile areas and contribute to the planning of regional sustainable development. At the same time, this method is also transferable to areas where LU changes drastically under intensive human activities, including basins, coastal zones and urban agglomerations.

Author contributions

Zhenyu Shen and Yafei Wang designed the study, processed and analyzed the data, prepared figures, and wrote the draft of the manuscript. Han Su, Yao He and Shuang Li contributed to the formal analysis, writing and the final form of the manuscript. All authors have read and agreed on the published version of the manuscript.

Declaration of competing interest

The authors declare that they have no known competing financial interests or personal relationships that could have appeared to influence the work reported in this paper.

Acknowledgements

This work was supported by the Second Tibetan Plateau Scientific Expedition and Research Program (2019QZKK0406), the Strategic Priority Research Program of the Chinese Academy of Sciences (XDA20020301), and a grant from State Key Laboratory of Resources and Environmental Information System.We are also grateful to Gao Xiaohong's team from Qinghai Normal University for their previous field survey and support of part of the sample collection.

References

Atkinson, P.M., Jeganathan, C., Dash, J., Atzberger, C., 2012. Inter-comparison of four models for smoothing satellite sensor time-series data to estimate vegetation phenology. Remote Sens. Environ. 123, 400–417. https://doi.org/10.1016/j.rse.2012.04.001.

Beaton, A., Whaley, R., Corston, K., Kenny, F., 2019. Identifying historic river ice breakup timing using MODIS and Google Earth Engine in support of operational flood monitoring in Northern Ontario. Remote Sens. Environ. 224, 352–364. https://doi.org/10.1016/j.rse.2019.02.011.

Belgiu, M., Drăguţ, L., 2016. Random forest in remote sensing: a review of applications and future directions. ISPRS J. Photogrammetry Remote Sens. 114, 24–31. https://doi.org/10.1016/j.isprsjprs.2016.01.011.

Bhosle, K., Musande, V., 2019. Evaluation of deep learning CNN model for land use land cover classification and crop identification using hyperspectral remote sensing images. J. Indian. Soc. Rem. Sens. 47 (11), 1949–1958. https://doi.org/10.1007/s12524-019-01041-2.

Bruzzone, L., Prieto, D.F., 2000. An adaptive parcel-based technique for unsupervised change detection. Int. J. Rem. Sens. 21 (4), 817–822.

Cao, X., Gao, X., Shen, Z., Li, R., 2020. Expansion of Urban Impervious Surfaces in Xining City Based on GEE and Landsat Time Series Data. IEEE Access. https://doi.org/10.1109/ACCESS.2020.3013640.

Chai, B., Li, P., 2018. Annual urban expansion extraction and spatio-temporal analysis using landsat time series data: a case study of tianjin, China. IEEE J. Sel. Topics Appl. Earth Observ. 11 (8), 2644–2656. https://doi.org/10.1109/JSTARS.2018.2829525.

Chen, Z., Wang, G., Pan, Y., Yang, X., Shen, Y., 2021a. Water use patterns differed notably with season and slope aspect for Caragana korshinskii on the Loess Plateau of China. Catena 198. https://doi.org/10.1016/j.catena.2020.105028.

Chen, B., Xu, B., Gong, P., 2021b. Mapping essential urban land use categories (EULUC) using geospatial big data: progress, challenges, and opportunities. Big Earth Data 5 (3), 410–441. https://doi.org/10.1080/20964471.2021.1939243.

Coppin, P., Jonckheere, I., Nackaerts, K., Muys, B., Lambin, E., 2010. Review ArticleDigital change detection methods in ecosystem monitoring: a review. Int. J. Rem. Sens. 25 (9), 1565–1596. https://doi.org/10.1080/0143116031000101675.

Cracknell, A.P., 2019. The development of remote sensing in the last 40 years. Int. J. Rem. Sens. 39 (23), 8387–8427. https://doi.org/10.1080/01431161.2018.1550919.

Cui, F., Wang, B., Zhang, Q., Tang, H., De Maeyer, P., Hamdi, R., Dai, L., 2021. Climate change versus land-use change-What affects the ecosystem services more in the forest-steppe ecotone? Sci.Tot.Environ. 759 https://doi.org/10.1016/j.scitotenv.2020.143525.

Dong, B.Q., Qin, T.L., Wang, Y., Zhao, Y., Liu, S.S., Feng, J.M., Zhang, X., 2021. Spatiotemporal variation of nitrogen and phosphorus and its main influencing factors in Huangshui River basin. Environ. Monit. Assess. 193 (5) https://doi.org/10.1007/s10661-021-09067-1.

Farr, T.G., Rosen, P.A., Caro, E., Crippen, R., Duren, R., Hensley, S., Kobrick, M., Paller, M., Rodriguez, E., Roth, L., Seal, D., Shaffer, S., Shimada, J., Umland, J., Werner, M., Oskin, M., Burbank, D., Alsdorf, D.E., 2007. The shuttle radar topography mission. Rev. Geophys. 45 (2) https://doi.org/10.1029/2005RG000183. RG2004.

Feizizadeh, B., Kazamei, Garajeh, M., Blaschke, T., Lakes, T., 2021a. A deep learning convolutional neural network algorithm for detecting saline flow sources and mapping the environmental impacts of the Urmia Lake drought in Iran. Catena 105585.

Feizizadeh, B., Mohmmadzadeh Alajujeh, K., Lakes, T., Blaschke, T., Omarzadeh, D., 2021b. A comparative approach of integrated fuzzy object-based deep learning and machine learning techniques for monitoring land use/cover changes and environmental impacts assessment. GIScince and remote sesning. https://doi.org/10.1080/15481603.2021.2000350.

Feizizadeh, B., Omarzadeh, D., Kazamei, Garajeh, M., Lakes, T., Blaschke, T., Omarzadeh, D., 2021c. Machine learning data-driven approaches for land use/cover mapping and trend analysis using Google Earth Engine. J. Environ. Plann. Manag. https://doi.org/10.1080/09640568.2021.2001317.

Foody, G.M., Mathur, A., 2004. Toward intelligent training of supervised image classifications: directing training data acquisition for SVM classification. Remote Sens. Environ. 93 (1–2), 107–117. https://doi.org/10.1016/j.rse.2004.06.017.

Franklin, S.E., 2020. Interpretation and use of geomorphometry in remote sensing: a guide and review of integrated applications. Int. J. Rem. Sens. 41 (19), 7700–7733. https://doi.org/10.1080/01431161.2020.1792577.

Garajeh, M.K., Malakyar, F., Weng, Q., Feizizadeh, B., Blaschke, T., Lakes, T., 2021. An automated deep learning convolutional neural network algorithm applied for soil salinity distribution mapping in Lake Urmia, Iran. Sci. Total Environ. 778, 146253.

Ge, J., Zhang, X., 2017. Temporal and spatial variation characteristics of temperature and precipitation in Huangshui basin, Qinghai. J. Irrig. Drain. 36 (11), 94–100.

Gorelick, N., Hancher, M., Dixon, M., Ilyushchenko, S., Thau, D., Moore, R., 2017. Google Earth engine: planetary-scale geospatial analysis for everyone. Remote Sens. Environ. 202, 18–27. https://doi.org/10.1016/j.rse.2017.06.031.

Grings, F., Roitberg, E., Barraza, V., 2020. EVI time-series breakpoint detection using convolutional networks for online deforestation monitoring in chaco forest. IEEE Trans. Geosci. Remote Sens. 58 (2), 1303–1312. https://doi.org/10.1109/tgrs.2019.2945719.

Hu, Y., Hu, Y., 2019. Land cover changes and their driving mechanisms in Central Asia from 2001 to 2017 supported by google earth engine. Remote Sens. https://doi.org/10.3390/rs11050554.

Hu, X., Zhang, H., Hao, H., Feng, D., Liu, H., Zhang, Q., 2020. Understanding the relationships between poverty alleviation and ecosystem conservation: empirical

evidence from western China. Front. Earth Sci. 14 (1), 209–220. https://doi.org/10.1007/s11707-019-0764-x.
Hütt, C., Koppe, W., Miao, Y., Bareth, G., 2016. Best accuracy land use/land cover (LULC) classification to derive crop types using multitemporal, multisensor, and multi-polarization SAR satellite images. Rem. Sens. 8 (8) https://doi.org/10.3390/rs8080684.
Ibrahim, W.Y., Batzli, S., Menzel, W.P., 2014. Agricultural policy effects on land cover and land use over 30 years in Tartous, Syria, as seen in Landsat imagery. J. Appl. Remote Sens. 8 (1) https://doi.org/10.1117/1.Jrs.8.083506.
Jia, J., Ma, G., Qin, C., Wang, L., 2020. Place-based policies, state-led industrialisation, and regional development: evidence from China's Great Western Development Programme. Eur. Econ. Rev. 123 https://doi.org/10.1016/j.euroecorev.2020.103398.
Jin, Y., Liu, X., Chen, Y., Liang, X., 2018. Land-cover mapping using Random Forest classification and incorporating NDVI time-series and texture: a case study of central Shandong. Int. J. Rem. Sens. 39 (23), 8703–8723. https://doi.org/10.1080/01431161.2018.1490976.
Jin, Y., Liu, X., Yao, J., Zhang, X., Zhang, H., 2019. Mapping the annual dynamics of cultivated land in typical area of the Middle-lower Yangtze plain using long time-series of Landsat images based on Google Earth Engine. Int. J. Rem. Sens. 41 (4), 1625–1644. https://doi.org/10.1080/01431161.2019.1673917.
Khanal, N., Matin, M.A., Uddin, K., Poortinga, A., Chishtie, F., Tenneson, K., Saah, D., 2020. A comparison of three temporal smoothing algorithms to improve land cover classification: a case study from Nepal. Rem. Sens. 12 (18) https://doi.org/10.3390/rs12182888.
Lee, J.S.H., Wich, S., Widayati, A., Koh, L.P., 2016. Detecting industrial oil palm plantations on Landsat images with Google Earth Engine. Rem. Sens. Applic. Soc. Environ. 4, 219–224. https://doi.org/10.1016/j.rsase.2016.11.003.
Li, X., Gong, P., Liang, L., 2015. A 30-year (1984-2013) record of annual urban dynamics of Beijing City derived from Landsat data. Remote Sens. Environ. 166, 78–90. https://doi.org/10.1016/j.rse.2015.06.007.
Li, H., Jia, M., Zhang, R., Ren, Y., Wen, X., 2019a. Incorporating the plant phenological trajectory into mangrove species mapping with dense time series sentinel-2 imagery and the Google Earth engine. Platform. Rem. Sens. 11 (21) https://doi.org/10.3390/rs11212479.
Li, H., Wan, W., Fang, Y., Zhu, S., Chen, X., Liu, B., Hong, Y., 2019b. A Google Earth Engine-enabled software for efficiently generating high-quality user-ready Landsat mosaic images. Environ. Model. Software 112, 16–22. https://doi.org/10.1016/j.envsoft.2018.11.004.
Liu, X., Hu, G., Chen, Y., Li, X., Xu, X., Li, S., Wang, S., 2018. High-resolution multi-temporal mapping of global urban land using Landsat images based on the Google Earth Engine Platform. Remote Sens. Environ. 209, 227–239. https://doi.org/10.1016/j.rse.2018.02.055.
Long, J., Liu, Y., Xing, S., Qiu, L., Huang, Q., Zhou, B., Zhang, L., 2018. Effects of sampling density on interpolation accuracy for farmland soil organic matter concentration in a large region of complex topography. Ecol.Indec. 93, 562–571. https://doi.org/10.1016/j.ecolind.2018.05.044.
Mahdianpari, M., Salehi, B., Mohammadimanesh, F., Homayouni, S., Gill, E., 2019. The first wetland inventory map of newfoundland at a spatial resolution of 10 m using sentinel-1 and sentinel-2 data on the Google Earth engine cloud computing platform. Rem. Sens. 11 (1) https://doi.org/10.3390/rs11010043.
McNally, A., Arsenault, K., Kumar, S., Shukla, S., Peterson, P., Wang, S., Funk, C., Peters-Lidard, C.D., Verdin, J.P., 2017. A land data assimilation system for sub-Saharan Africa food and water security applications. Sci. Data 4, 170012.
Mountrakis, G., Im, J., Ogole, C., 2011. Support vector machines in remote sensing: a review. ISPRS J. Photogrammetry Remote Sens. 66 (3), 247–259.
Mutanga, O., Kumar, L., 2019. Google Earth engine applications. Rem. Sens. 11 (5) https://doi.org/10.3390/rs11050591.
Nyland, E., Gunn, K.E., Shiklomanov, G.I., Engstrom, N.N., R, Streletskiy, A., D, 2018. Land cover change in the lower yenisei river using dense stacking of landsat imagery in Google Earth engine. Rem. Sens. 10 (8) https://doi.org/10.3390/rs10081226.
Peng, W., Lopez-Carr, D., Wu, C., Wang, X., Longcore, T., 2020. What factors in fluence the willingness of protected area communities to relocate? China's ecological relocation policy for Dashanbao Protected Area. Sci.Tot.Environ. 727 https://doi.org/10.1016/j.scitotenv.2020.138364.
Sazib, N., Mladenova, I., Bolten, J., 2018. Leveraging the Google Earth engine for drought assessment using global soil moisture data. Rem. Sens. 10 (8) https://doi.org/10.3390/rs10081265.
Shao, Y., Lunetta, R.S., Wheeler, B., Iiames, J.S., Campbell, J.B., 2016. An evaluation of time-series smoothing algorithms for land-cover classifications using MODIS-NDVI multi-temporal data. Remote Sens. Environ. 174, 258–265. https://doi.org/10.1016/j.rse.2015.12.023.
Smits, P.C., Annoni, A., 2000. Towards specification-driven change detection. IEEE Trans. Geosci. Rem. Sens. 38, 1484–1488.
Teluguntla, P., Thenkabail, P.S., Oliphant, A., Xiong, J., Gumma, M.K., Congalton, R.G., Huete, A., 2018. A 30-m landsat-derived cropland extent product of Australia and China using random forest machine learning algorithm on Google Earth Engine cloud computing platform. ISPRS J. Photogrammetry Remote Sens. 144, 325–340. https://doi.org/10.1016/j.isprsjprs.2018.07.017.
Thyagharajan, K.K., Vignesh, T., 2017. Soft computing techniques for land use and land cover monitoring with multispectral remote sensing images: a review. Arch. Comput. Methods Eng. 26 (2), 275–301. https://doi.org/10.1007/s11831-017-9239-y.
Tian, H., Banger, K., Bo, T., Dadhwal, V.K., 2014. History of land use in India during 1880–2010: large-scale land transformations reconstructed from satellite data and historical archives. Global Planet. Change 121, 78–88. https://doi.org/10.1016/j.gloplacha.2014.07.005.
Tsai, Y.H., Stow, D., Chen, H.L., Lewison, R., An, L., Shi, L., 2018. Mapping vegetation and land use types in fanjingshan national nature reserve using Google Earth engine. Rem. Sens. 10 (6) https://doi.org/10.3390/rs10060927.
Turner, B.L., II Lambin, E.F., Reenberg, A., 2007. The emergence of land change science for global environmental change and sustainability. Proc. Natl. Acad. Sci. U.S.A. 104 (52), 20666–20671. https://doi.org/10.1073/pnas.0704119104.
Verbesselt, J., Hyndman, R., Newnham, G., Culvenor, D., 2010. Detecting trend and seasonal changes in satellite image time series. Remote Sens. Environ. 114 (1), 106–115.
Wang, R., Gamon, J.A., 2019. Remote sensing of terrestrial plant biodiversity. Remote Sens. Environ. 231 https://doi.org/10.1016/j.rse.2019.111218.
Wang, Y., Zhao, F., Chen, P., 2017. A framework of spatiotemporal fuzzy clustering for land-cover change detection using SAR time series. Int. J. Rem. Sens. 38 (2), 450–466. https://doi.org/10.1080/01431161.2016.1268736.
Weiss, M., Jacob, F., Duveiller, G., 2020. Remote sensing for agricultural applications: a meta-review. Remote Sens. Environ. 236 https://doi.org/10.1016/j.rse.2019.111402.
Wu, Y., Zhang, P., Wu, J., Li, C., 2021. Object-oriented and deep-learning-based high-resolution mapping from large remote sensing imagery. J.Can. Rem. Sens. 47 (3), 396–412. https://doi.org/10.1080/07038992.2021.1944802.
Xie, S., Liu, L., Zhang, X., Yang, J., Chen, X., Gao, Y., 2019. Automatic land-cover mapping using landsat time-series data based on Google Earth engine. Rem. Sens. 11 (24), 3023. https://doi.org/10.3390/rs11243023.
Xu, X., Zhang, Y. China Meteorological Background Dataset. Data Registration and Publishing System of the Resource and Environmental Science Data Center of the Chinese Academy of Sciences.
Xu, Y., Qiu, X., Yang, X., Lu, X., Chen, G., 2020. Disaster risk management models for rural relocation communities of mountainous southwestern China under the stress of geological disasters. Int. J. Disaster Risk Reduc. 50 https://doi.org/10.1016/j.ijdrr.2020.101697.
Yang, F., Liu, Q., 2013. Temporal and spatial distribution characteristics of long-term variation trend of precipitation in Huangshui basin and its relationship with temperature. J. N.W.T. Univ. Agric. For. Sci. Technol. 41 (5), 201–206.
Yang, Z., Li, J., Shen, Y., Miao, H., Yan, X., 2018. A denoising method for inter-annual NDVI time series derived from Landsat images. Int. J. Rem. Sens. 39 (12), 3816–3827.
Zeng, L., Wardlow, B.D., Xiang, D., Hu, S., Li, D., 2020. A review of vegetation phenological metrics extraction using time-series, multispectral satellite data. Remote Sens. Environ. 237 https://doi.org/10.1016/j.rse.2019.111511.
Zhang, L., Weng, Q., 2016. Annual dynamics of impervious surface in the Pearl River Delta, China, from 1988 to 2013, using time series Landsat imagery. ISPRS J. Photogrammetry Remote Sens. 113, 86–96. https://doi.org/10.1016/j.isprsjprs.2016.01.003.
Zhang, F., Yang, X., 2020. Improving land cover classification in an urbanized coastal area by random forests: the role of variable selection. Remote Sens. Environ. 251 https://doi.org/10.1016/j.rse.2020.112105.
Zhang, L., Weng, Q., Shao, Z., 2017. An evaluation of monthly impervious surface dynamics by fusing Landsat and MODIS time series in the Pearl River Delta, China, from 2000 to 2015. Remote Sens. Environ. 201, 99–114. https://doi.org/10.1016/j.rse.2017.08.036.
Zhang, W., Wang, L., Xiang, F., Qin, W., Jiang, W., 2020. Vegetation dynamics and the relations with climate change at multiple time scales in the Yangtze River and Yellow River Basin, China. Ecol.Indec. 110 https://doi.org/10.1016/j.ecolind.2019.105892.
Zhao, Y., Li, M., Wang, X., Deng, J., Zhang, Z., Wang, B., 2020. Influence of habitat on the phylogenetic structure of Robinia pseudoacacia forests in the eastern Loess Plateau, China. Glob.Ecol.Conser. 24, e01199 https://doi.org/10.1016/j.gecco.2020.e01199.